

# Fano-Resonant, Asymmetric, Metamaterial-Assisted Tweezers for Single Nanoparticle Trapping

Domna G. Kotsifaki, Viet Giang Truong, and Síle Nic Chormaic\*

*Light-Matter Interactions for Quantum Technologies Unit, Okinawa Institute of Science  
and Technology Graduate University, Onna-son, Okinawa, 904-0495, Japan*

E-mail: [sile.nicchormaic@oist.jp](mailto:sile.nicchormaic@oist.jp); [v.g.truong@oist.jp](mailto:v.g.truong@oist.jp)

## Abstract

Plasmonic nanostructures overcome Abbe's diffraction limit to create strong gradient electric fields, enabling efficient optical trapping of nanoparticles. However, it remains challenging to achieve stable trapping with low incident laser intensity. Here, we demonstrate a Fano resonance-assisted plasmonic optical tweezers for single nanoparticle trapping in an array of asymmetrical split nano-apertures on a 50-nm gold thin film. A large normalized trap stiffness of 8.65 fN/nm/mW for 20 nm polystyrene particles at a near-resonance trapping wavelength of 930 nm was achieved. The trap stiffness on-resonance is enhanced by a factor of 63 compared to off-resonance due to the ultrasmall mode volume, enabling large near-field strengths and a cavity Purcell effect contribution. These results facilitate trapping with low incident laser intensity, thereby providing new options for studying transition paths of single molecules such as proteins.

**Keywords:** Fano resonance, Metamaterial, Plasmonic tweezers, Nanoparticle trapping, Stiffness enhancement.

# Introduction

Metallic nanostructures have attracted considerable attention for enhancing light-matter interactions due to unique properties that enable them to concentrate light beyond the diffraction limit, thereby enabling strong field confinement.<sup>1,2</sup> By patterning metal nanostructures in arrays,<sup>2,3</sup> one can achieve lower radiation losses, higher quality factors, and large field enhancements over wide effective cross-sections, all characteristics that are important for a variety of applications. Various nanostructure arrays have been fabricated to achieve ultra-sensitive biodetection,<sup>4,5</sup> to create advanced liquid crystal devices,<sup>6</sup> to crystallize proteins,<sup>7</sup> to deliver drugs,<sup>8</sup> to monitor cancer<sup>9</sup> and to perform biomedical imaging.<sup>10</sup>

Likewise, plasmonic optical tweezers (POTs)<sup>11–15</sup> provide a label-free method of single-nanoparticle characterization<sup>16–21</sup> and contribute to the development of lab-on-chip analytical platforms. Typically, POTs rely on evanescent waves around metallic nanostructures, which produce localized intensities that enhance optical forces at the nanoscale. For example, Roxworthy et al.<sup>22</sup> introduced an array trapping platform to control single-particle and multi-particle trapping by adjusting the trapping incident power. The authors claimed that their device opened the door for specific particle trapping selectivity based upon size, mass, and/or refractive index. However, in some cases where manipulation of temperature-sensitive bioparticles is needed, nano-aperture based POTs, which enable stable trapping with low incident intensity, are used,<sup>16,18,19,23–25</sup> thereby minimizing phototoxicity.<sup>25</sup> By arraying nano-aperture units<sup>16,22,26,27</sup> in metallic substrates, many trapping sites can be activated at the same time, permitting simultaneous analysis of several particles locally trapped in well-defined positions of the plasmonic nanostructure and providing an alternative method for particle crystallization. Therefore, selectivity of biomolecule trapping in a heterogeneous environment could have a significant impact on defining structural information during transition paths,<sup>28</sup> leading, among other things, to more precise drug design.<sup>29,30</sup>

Currently, metamaterials are being widely studied owing to their exceptional properties, which originate from structuring on a sub-wavelength scale.<sup>31–34</sup> In particular, they pave the

way for a new world of remarkable applications, including slow light devices,<sup>35</sup> cloaking,<sup>36</sup> and lasing spasers.<sup>37,38</sup> Fano-resonant, asymmetric, split-ring metamaterials exhibit sharp resonances caused by interference between super-radiant and subradiant plasmonic modes.<sup>39,40</sup> By exploiting Fano resonances, it is possible to confine light more efficiently, characterized by a steeper dispersion than the dipole resonance. Owing to their extreme sensitivity to local geometrical changes, they have been proposed as a quantitative biosensing platform where the Fano resonance shows sensitivity for protein recognition.<sup>34</sup> Additionally, a Fano metamaterial consisting of a disc-double, split-ring resonator enhances the chiral gradient force on sub-10-nm enantiomers, enabling new options for chiral trapping and separation.<sup>41</sup> The fact that the Fano resonance peak is highly sensitive to modifications of its surrounding medium<sup>32</sup> renders metamaterials particularly attractive for stable optical trapping applications.

In this work, we introduce a novel approach for strong, single-nanoparticle trapping, based on Fano resonance-assisted plasmonic optical tweezers (FAPOT). To the best of our knowledge, this is the first experimental demonstration of a FAPOT metamaterial for nanoparticle trapping. This approach provides superior stable plasmonic trapping for nanoscale particles, demonstrating enhanced trapping performance with near-infrared wavelength tunability. We fabricated an array of asymmetric, split-ring (ASR) plasmonic nanostructures that were used as trapping substrates. We studied the trapping performance via power- and wavelength-dependent characterization, revealing the highest effective trap stiffness reported to date for 20 nm polystyrene (PS) nanoparticles, equal to 8.65 fN/nm/mW under resonance conditions. We experimentally investigated polarization-dependent properties of the metamaterial via trap stiffness measurements. We conclude that the ability of our system/platform to perform steady and dynamic optical manipulation makes a variety of lab-on-chip applications possible.

# Results

Figure 1a is a scanning electron microscope (SEM) image of 4x4 ASR metamolecules at an angle of  $52^\circ$  from the surface normal. The experimental set-up used in this work (Figure S1 in the Supporting Information-SI) is based on an inverted microscope. From recorded images, we estimated that the laser spot size at the objective focus was approximately  $2.0\ \mu\text{m}$  and the number of units that could be illuminated on the array was  $5 \times 5$ , *i.e.*, 25 metamolecules. According to Fedotov et al.<sup>42</sup> the quality factor,  $Q$ -factor (see SI) of the ASR metamaterial strongly depends on the size of the illuminated area, *i.e.*, the total number of ASR units involved in the interaction with the incident light. Thus, the more ASR units exposed to the incident laser beam, the more the material losses (*i.e.*, Ohmic losses in the metal and dissipation losses in the glass substrate) and radiation losses are reduced.<sup>42</sup> As a result, the number of ASR units illuminated by the trapping laser beam ensures a high  $Q$ -factor of the metamaterial<sup>42</sup> and a narrow Fano resonance peak under resonance conditions.

Figure 1b shows the transmission spectra of the ASR metamaterial in deionized water as a function of the polarization angle. For vertical polarization (*i.e.*,  $90^\circ$  gray line in Figure 1b), the metamaterial device did not show spectral features originating from asymmetrical structuring. Note that the transmission spectrum difference between the two orthogonal polarizations implies that this metamaterial can be used to improve detection sensitivity for horizontal polarization, *i.e.*, at  $0^\circ$ . Figure 1c shows the measured spectra for transmission, reflection, and absorption of the ASR metamaterial in deionized water for horizontal polarization. The absorption peak of the ASR metamaterial appears at 928 nm and represents the closed-mode Fano-type excitation. The mode is formed by collective interactions between individual metamolecules and this justifies the major characteristics required for the particle trap stiffness enhancement in our work.

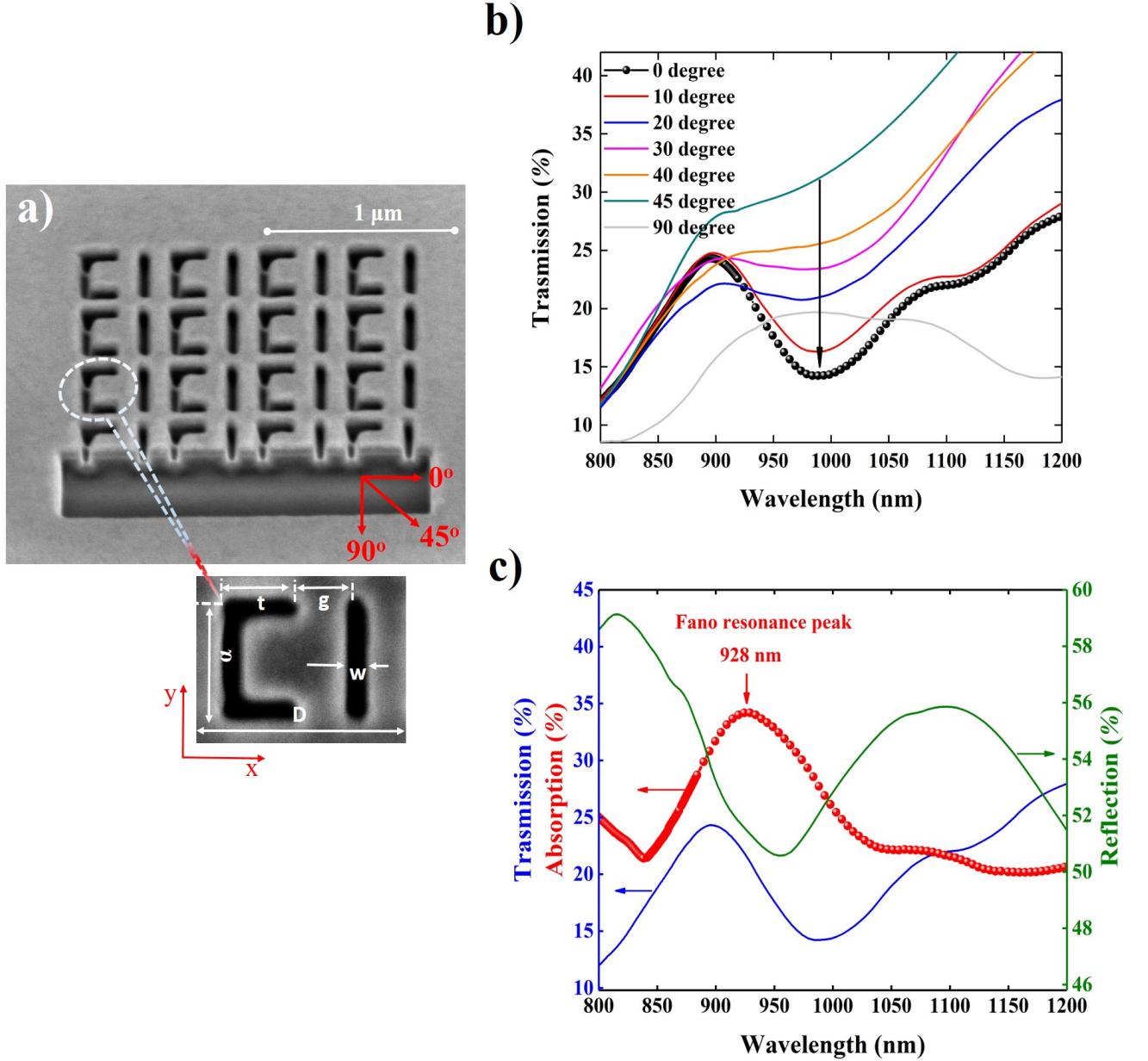


Figure 1: (a) Scanning electron microscope (SEM) image, viewed at  $52^\circ$  from the surface normal. The metamaterial structure is a  $4 \times 4$  array of ASR metamolecules in a 50-nm gold thin film. Zoom: Metamolecule unit with feature dimensions:  $D = 400.0 \pm 2.1$  nm, vertical slit  $\alpha = 310.0 \pm 1.3$  nm, horizontal slit  $t = 164.4 \pm 2.6$  nm, gap  $g = 101.3 \pm 3.2$  nm and slit width  $w = 44.3 \pm 1.8$  nm. (b) Transmission spectra featuring the resonance of an array of 36 metamolecules ( $6 \times 6$  units) of the metamaterial in deionized water versus the polarization angle of the microspectrophotometer light source. The arrow indicates resonance changes. (c) Transmission (blue solid line), reflection (green solid line), and absorption (red symbol-line) spectra of an array of 36 units of the metamaterial in deionized water at  $0^\circ$  polarization angle of the microspectrophotometer light source. The Fano resonance peak appears at 928 nm (vertical red arrow).

Figure 2 shows a raw data trace of the avalanche photodiode (APD) signal versus time. The trapping wavelength was 910 nm and the trapping laser intensity was  $0.96 \text{ mW}/\mu\text{m}^2$  at the sample plane. When a PS particle approaches excited ASRs, the optical gradient force pulls the particle toward the nano-aperture of the ASR metamaterial. Figure 2a shows the cycle of trapping and releasing of a 20 nm PS particle in an array of ASRs. As the PS particle was trapped, APD signals were recorded and, subsequently, the laser was blocked to release the trapped particle from the nanostructure. After 7 sec, we re-illuminated the metamaterial, leading to another step-like signal showing nearly identical trap and release intensity levels. This reversible trap/release cycle was repeated several times demonstrating the high repeatability of the trapping process. Figure 2b shows a single step-like jump in the APD signal, typically within 1 min. Fluctuations in the APD signal correspond to the Brownian motion of the particle in the trap. By changing the trapping laser power and the trapping time duration, we observed multiple nanoparticle trapping events (Figure S2-SI). However, in our work, in order to determine the trap stiffness enhancement factor, we only analyze data for the first observable single-nanoparticle trapping event.

For small displacements (*i.e.*,  $|x| \ll \lambda$ , where  $\lambda$  is the trapping wavelength)<sup>18</sup> of the particle from the trap, the overdamped Langevin equation<sup>18</sup> can be applied:

$$\gamma \dot{x}(t) + \kappa_{tot} x(t) = \xi(t), \quad (1)$$

where  $\gamma$  is the viscous damping,  $x(t)$  the displacement of the particle from the equilibrium point,  $\kappa_{tot}$  the total trap stiffness, which is proportional to the trapping laser intensity, and  $\xi(t)$  is the thermal fluctuation. Using an exponential fit of the trapping transient region, the trap stiffness,  $\kappa_{tot}$ , is determined from the following:<sup>17</sup>

$$\tau = \frac{\gamma}{\kappa_{tot}}, \quad (2)$$

where  $\tau$  is the exponential decay time. To validate our trap stiffness observations evaluated

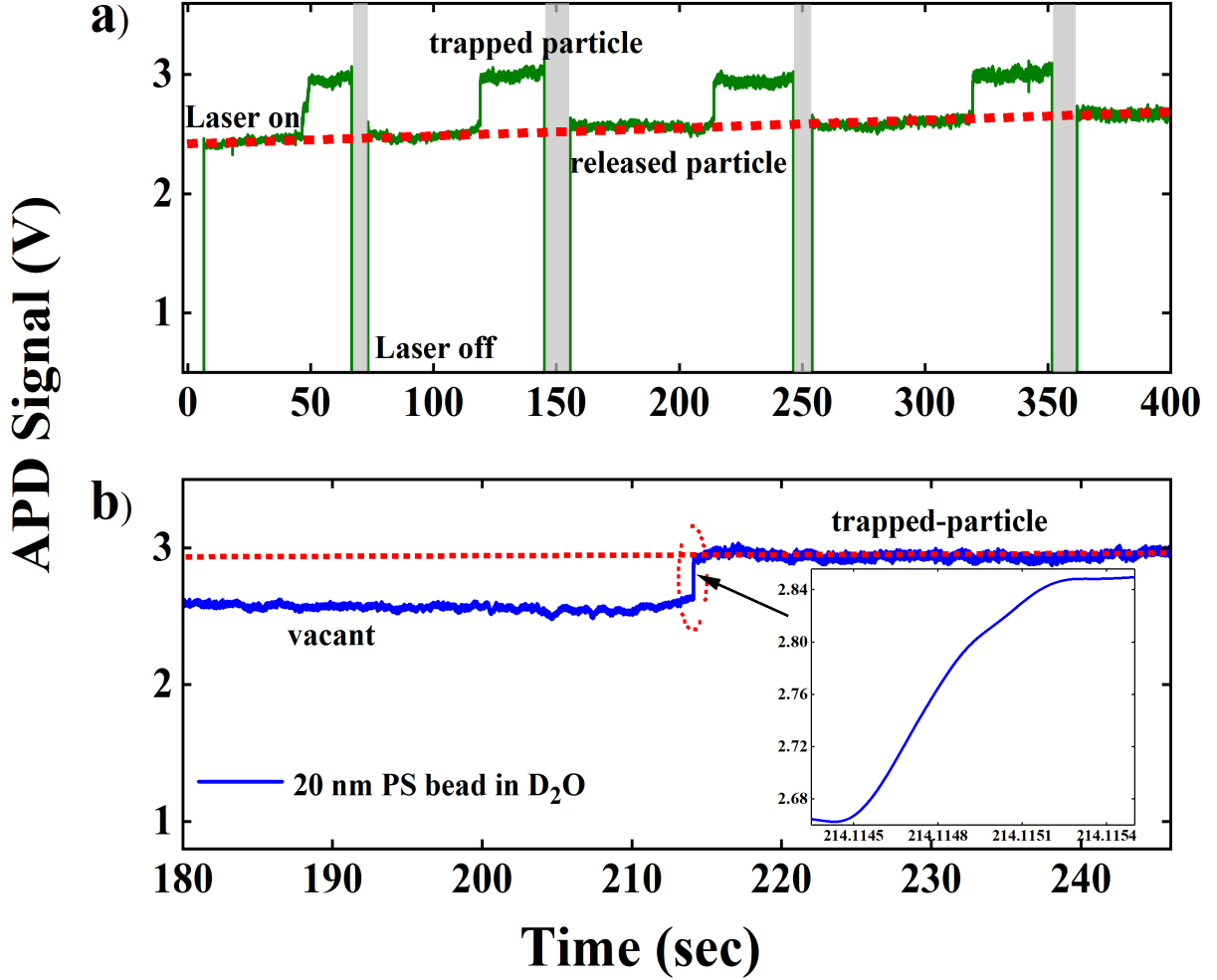


Figure 2: (a) Time trace of the APD signal through the ASR metamaterial in heavy water containing suspended 20 nm PS particles as a function of the trapping laser beam for a trapping laser wavelength of 910 nm. Gray regions indicate times when the laser was blocked, triggering release of the trapped PS particle. (b) Time trace of a typical trapping event of a 20 nm PS particle. Inset: a zoom of the trapping event at 214.1 sec, representing a time interval of 0.9 ms. The trapping laser intensity at the sample plane was  $0.96 \text{ mW}/\mu\text{m}^2$ .

using the time constant of the particle's thermal motion method, we further analyzed the trap stiffness for a single nanoparticle, for both on-resonance and off-resonance wavelengths, using the power spectral density (PSD) method from recorded transmission data *i.e.*, the APD signal (see S3-SI). We conclude that the transient method is the most suitable method to analyze our data for single nanoparticle trapping events. For the trap stiffness calculation, the effective distance between the 20 nm PS particle and the surface of the ASR wall is 5

nm.<sup>16,17</sup> This is due to the surface roughness of the fabricated ASR device. We consider the Stokes' drag coefficient and adjust it using Faxen's correction factor for the trap stiffness calculations (see S4-SI). Thence, the trap stiffness increases by a factor of 1.78<sup>16,17</sup> (see Eq.S1-SI).

Figure 3 shows the trap stiffness as a function of the trapping laser intensity ranging from 0.23 mW/ $\mu\text{m}^2$  to 1.4 mW/ $\mu\text{m}^2$  for a 20 nm PS particle. As expected, the linear dependence of the trap stiffness versus laser intensity is obvious at both 910 nm and 950 nm, with deviation from linearity as the wavelength approaches the resonance peak at 930 nm. We obtained a maximum trap stiffness,  $\kappa_{tot} = 1.99$  fN/nm, for the lowest laser intensity, 0.23 mW/ $\mu\text{m}^2$ , corresponding to a normalized value of 8.65 fN/nm/mW for a trapping laser intensity of 1 mW/ $\mu\text{m}^2$ . This normalized trap stiffness is the highest experimental value reported to date for dielectric nanoparticles. Enhancement of the trap stiffness is a feature of the Fano resonant effect of the metamaterial on the FAPOT trapping. To further investigate the origin of the trap stiffness enhancement, we studied the dependence of the trap stiffness on wavelength.

Figure 4a shows the trap stiffness as a function of trapping laser intensity and wavelength. For each intensity value, data are fitted with a Lorentzian represented by the solid curve. For all fitting curves, we determined a resonance wavelength at  $931.36 \pm 1.76$  nm where the trap stiffness is maximal. The metamaterial's absorption resonance peak at 928 nm (Figure 1c) almost matches the experimentally obtained resonance trap stiffness peak, determined by Lorentzian fits to the trap stiffness data (Figure 4a) at 931 nm. Therefore, we conclude that the observed stiffness enhancement mainly arises from the enhanced  $Q$ -factor of the Fano-type surface plasmon resonance excitation. Moreover, we noticed that the full width at half maximum (FWHM) of the trap stiffness curve as a function of the trapping wavelength is approximately 14 nm, which is much narrower than that obtained for the absorption spectra of 105 nm (Figure 4b).

In Figure 4c, we plot the trap stiffness enhancement factor as a function of trapping



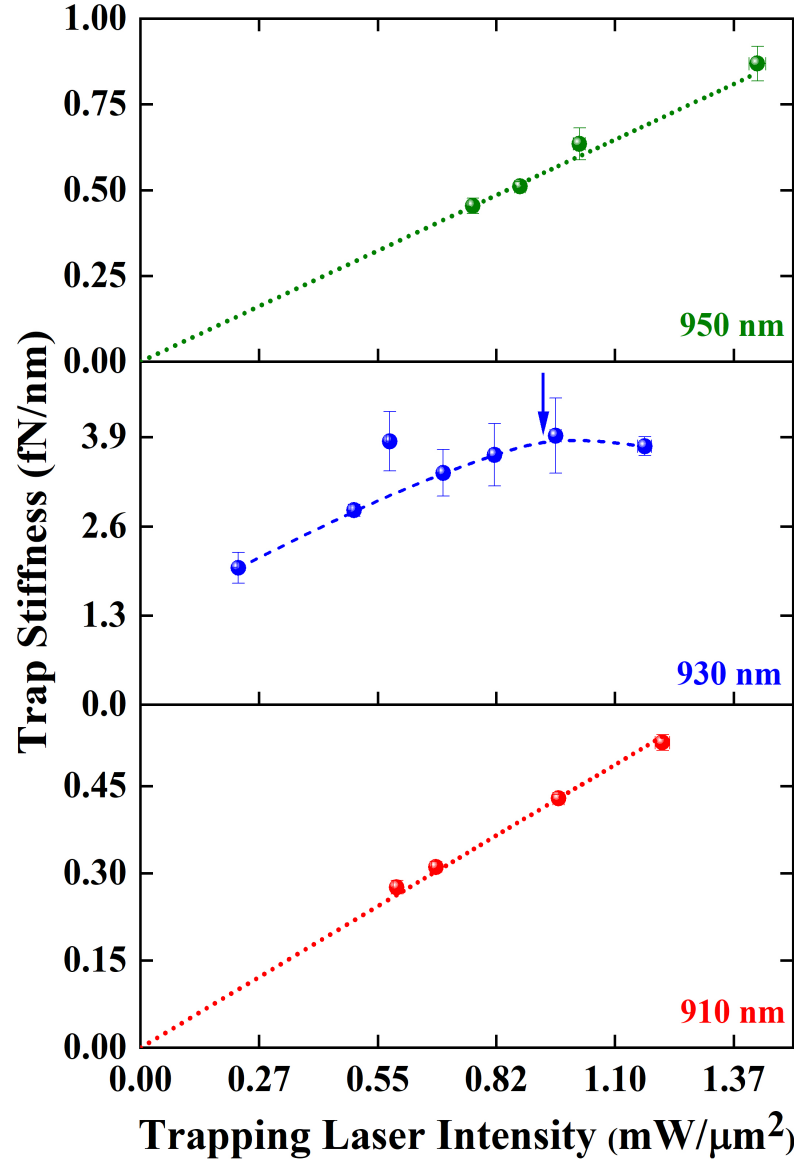


Figure 3: Trap stiffness of a single 20 nm PS particle as a function of incident laser intensity for laser trapping wavelengths of 950 nm, 930 nm, and 910 nm. Red and green dashed lines: Linear fit to the data obtained using the ASR metamaterial. The red dashed line has a slope of 0.16 [(fN/nm)/(mW/μm²)] and the green dashed line has a slope of 0.08 [(fN/nm)/(mW/μm²)]. The blue dashed line is a guide for the eye. The blue arrow indicates the point at which the data deviate from a linear trend. The  $y$ -error corresponds to the standard deviation of the trap stiffness measurements.

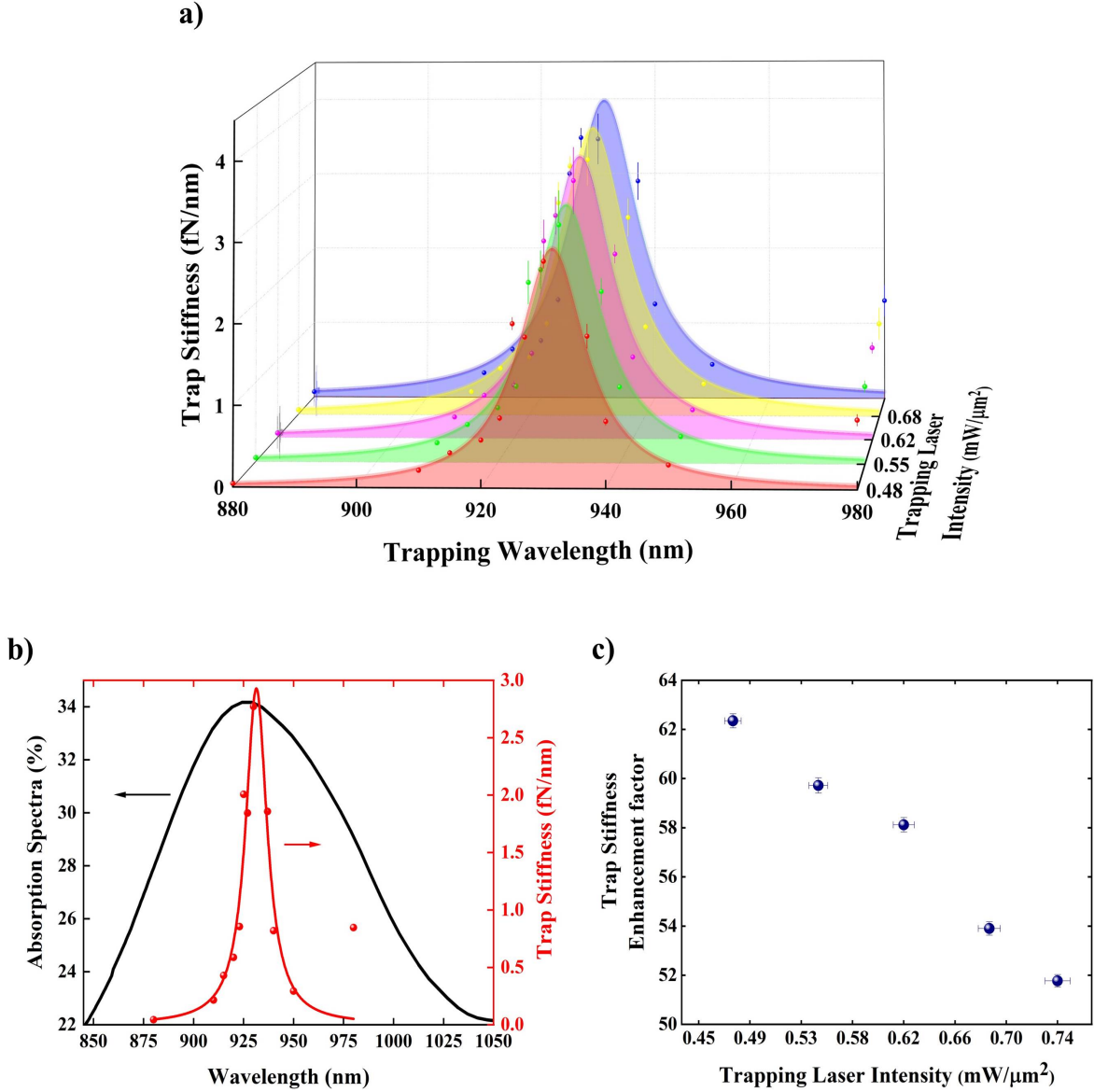


Figure 4: (a) Trap stiffness of a single 20 nm PS particle as a function of trap intensity and wavelength. The y-error corresponds to the standard deviation of the trap stiffness measurements. (b) Absorption spectrum and trap stiffness for a single 20 nm PS particle for a laser intensity of  $0.48 \text{ mW}/\mu\text{m}^2$  as a function of wavelength. (c) Trap stiffness enhancement factor as a function of incident trapping laser intensity. The trap stiffness enhancement is normalized to that measured at 880 nm, *i.e.*, far from the resonance peak. The *x*-error corresponds to the standard deviation of the power measurements and the *y*-error to the propagation error of the trap stiffness measurements.

laser intensity. The enhancement factor is normalized to the trap stiffness value obtained at 880 nm, *i.e.*, far from the Fano resonance peak. Interestingly, we note that a higher

trap stiffness enhancement is obtained for low trapping laser intensities and it diminishes as trapping intensity increases, indicating that the ASR metamaterial device is very sensitive to trapping laser intensity changes.

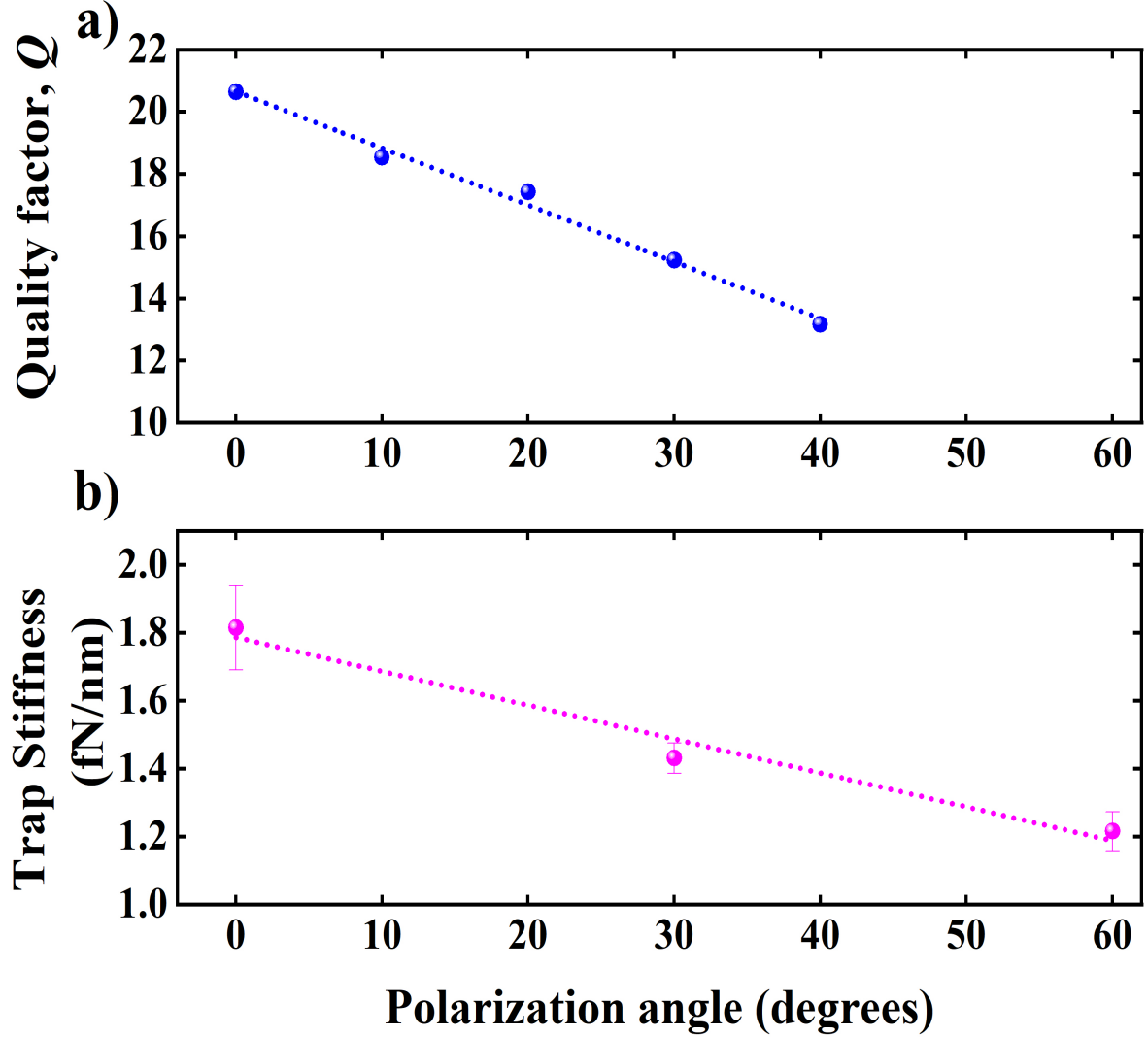


Figure 5: (a) Quality factor,  $Q$ , as a function of the polarization angle of the microspectrophotometer light source. The dashed line indicates the linear fit to the  $Q$ -factor data and has a slope of 0.18. (b) Trap stiffness for a single 20 nm PS particle as a function of polarization angle for a trapping wavelength of 937 nm and an intensity of  $0.82 \text{ mW}/\mu\text{m}^2$  at the sample position. The  $y$ -error corresponds to the standard deviation of the trap stiffness measurements. The dashed line indicates the linear fit to the trapping data and has a slope of 0.010 [(fN/nm)/degree].

Figure 5a is a plot of the  $Q$ -factor of the ASR metamaterial, as a function of polarization

angle of the microspectrophotometer light source. The  $Q$ -factor was calculated using Eq. S2 (see SI) based on data from Figure 1b. We could not calculate the  $Q$ -factor for angles larger than  $40^\circ$ . We observe that the  $Q$ -factor of the ASR metamaterial decreases as a function of polarization angle. This may imply that the net magnetic flux of the ASR metamaterial<sup>42</sup> vanishes due to non-efficient excitation of the resonance mode. Particularly, by changing the polarization of the incident light, interactions between individual ASR units mediated by the magneto-induced surface waves,<sup>42</sup> which contribute to excitation of the Fano resonance peak, are less strong, leading to an increase of scattering losses through magnetic dipole radiation.<sup>42</sup> Owing to the above-mentioned scattering loss analysis, we assume that the  $Q$ -factor diminishes as the polarization angle changes. Moreover, rotating the polarization reveals the difference in the near-field potential landscape experienced by the trapped PS particle, leading to a variation in the magnitude of the trap stiffness (Figure 5b). For a horizontal polarization ( $x$ -direction *or*  $0^\circ$  in Figure 1a), the Fano resonance dominates, whereas it vanishes for vertical polarization ( $y$ -direction *or*  $90^\circ$  in Figure 1a). The fact that the trap stiffness follows a similar trend as the  $Q$ -factor, confirms the exceptional polarization-dependent properties of the ASR metamaterial that modify its magnitude.

Finally, we performed numerical force calculations based on the Maxwell stress tensor using the COMSOL Multiphysics software package (S5-SI). We notice three different trapping potential depth regions are created within each ASR metamolecule. The optical force enhancement factor ranges from 6.5 to 20 times depending on the particle trapping location for on and off-resonance wavelengths. Therefore, we confirm that the enhancement of the experimental trap stiffness is mainly a feature of the Fano resonant effect of the ASR metamaterial.

# Discussion

In Table 1, we compare our experimentally measured trap stiffness for the ASR metamaterial with different nanotweezer systems reported in the literature.<sup>16,17,19,43–45</sup>

Table 1: **Trap stiffness for nanoscale optical tweezers**

Structure	Method	Trapping Wavelength (nm)	Nanoparticle (nm)	Trap Stiffness (fN/nm) to 1mW/ $\mu\text{m}^2$	Scaled Trap Stiffness <sup>a</sup> (fN/nm)
Silicon Nitride Photonic Crystal	exp. <sup>b</sup>	1064	22 PS	0.14	0.11
Silicon Nano-antennas	exp.	1064	20 PS	0.01	0.01
Double Nanohole	exp.	820	20 PS	0.10	0.10
Rectangular Nanocavity	sim. <sup>c</sup>	1064	20 PS	0.33	0.33
Coaxial Nano-apertures	sim.	692	10 (n = 2) <sup>d</sup>	0.19	1.56 (0.36) <sup>e</sup>
Connected Nano-aperture Array	exp.	980	30 PS	0.84	0.25
Asymmetric Split-Rings Metamaterial (this work)	exp.	930	20 PS	8.65	8.65

<sup>a</sup>  $(x10nm/r)^3$ , where  $r$  is the radius of the particle.

<sup>b</sup> experimental.

<sup>c</sup> simulation.

<sup>d</sup> an intermediate value between the refractive index of biomolecules and quantum dots.<sup>19</sup>

<sup>e</sup> scaled by the Clausius-Mossotti factor to the refractive index of polystyrene.

In the last column, trap stiffness has been scaled to a particle with a 10 nm radius, since the stiffness is proportional to the particle volume,<sup>46</sup> and to the Clausius-Massoti factor for the refractive index in the case of the coaxial nano-aperture. The coaxial nano-aperture width is comparable to the width of our ASR metamaterial device. Based on Table 1, ASR metamaterial structures demonstrate a scaled trap stiffness  $\sim 86$  times larger than that for a double nanohole and  $\sim 24$  times larger than that for a coaxial nano-aperture cavity. Moreover, we also compared our measured trap stiffness to those obtained for conventional optical tweezers,<sup>47</sup> using the same scaling methods without the contribution of Faxen’s correction factor (see S4-SI). In this case, the ASR metamaterial has a scaled trap stiffness of 4.86 fN/nm/mW for a 20 nm PS particle; this is 180 times larger than the stiffness of 0.027 fN/nm/mW obtained for a 220 nm particle<sup>47</sup> using conventional optical tweezers. Considering that the particle used in the conventional trapping scheme is 11 times larger than the particle used in our work, we conclude that the FAPOT is about  $10^5$  times more efficient than conventional optical trapping.

Recently, a plasmonic nanopore biosensor<sup>48</sup> was reported to hold and detect single molecules for extended trapping times in order to investigate perturbation of the molecule at hotspots. Even if this approach provides insights for precise nanotrapping optimization, the lack of augmented motion control of the biomolecule remains a challenge due to the weak trapping.<sup>48</sup> Therefore, a particularly stable trapping environment at low incident trapping laser intensity is mandatory to trap nanosized particles for extended measurement times. The high trap stiffness achieved in this work indicates the ability of our system to grab the particle efficiently, to pull it toward the hotspot, and to retain it there for a long time in order to study its structural characteristics and native dynamics. Therefore, our experimental trap stiffness magnitude is of fundamental importance for future understanding and exploitation of transition paths,<sup>28</sup> as well as investigations into the translocation mechanisms of biomolecules.<sup>49</sup>

The heating effect arising from gold’s absorption of the laser light can increase the Brownian motion of the trapped particle, thereby affecting the trap stiffness.<sup>25</sup> It has been reported that localized heating of the fluid (by illuminating metallic nano-apertures) can create a local gradient in the fluid density.<sup>50–52</sup> This intrinsic heating effect results in a drag force on the particle that moves it toward the hotspots where it will be trapped by the optical gradient forces.<sup>50–52</sup> Additionally, we have observed a nonlinear behavior in the trap stiffness for higher trapping light intensities (Figures 3), indicating possible localized heating of the surrounding medium when we use a near-resonance wavelength of 930 nm. This drag force could assist in the enhancement of the observed trap stiffness, presumably leading to a decrease in the FWHM of the trap stiffness resonance curve when compared to the FWHM of the absorption spectrum (Figure 4b).

To investigate the origin of the trap stiffness enhancement in our experiments, we assume that the particle is small enough and can be considered as a scattering point source at the resonant wavelength of 930 nm. We assume that scattered light from the particle coupling back into the ASR metamaterial may also participate in the modification of the trap stiffness.

We determine the Purcell factor,  $F_P$ , which allows us to estimate the coupling efficiency of a particle's scattered light, using the following:<sup>53</sup>

$$F_P = \frac{3}{4\pi^2} \left( \frac{\lambda_F}{n} \right)^3 \frac{Q}{V_{mod}}, \quad (3)$$

where  $Q$  is the quality factor (see Eq. S2-SI),  $V_{mod}$  is the mode volume (see Eq. S3-SI),  $\lambda_F = 928$  nm is the peak wavelength of the absorption spectrum in Figure 1c, and  $n = 1.33$  is the refractive index of the surrounding medium. Thence, we obtain a Purcell factor,  $F_P = 250$ . Subsequently, we estimate the enhancement factor,  $\mu$ , of the scattering light from the following:<sup>53</sup>

$$F_{p,exp} = \frac{\mu D^2 p}{V_{mod}}. \quad (4)$$

Considering that the theoretical FWHM of the trap potential along the  $x$ -direction is  $p = 50$  nm, we obtain a correction enhancement factor,  $\mu = 65.6$ . Interestingly, this observed Purcell enhancement factor of the scattered light is of the same order of magnitude as the particle's trap stiffness enhancement factor, *i.e.*,  $\mu = 62.4$  (Figure 4c). This significant enhancement of the trap stiffness and the estimated light scattered back into the ASR metamaterial arises from the strong interaction between the trapped nanoparticle and the surface plasmon metamaterial resonance.

Furthermore, in slow light devices such as photonic crystals<sup>54,55</sup> and metamaterials,<sup>56</sup> a decrease in the group velocity of the light corresponds to an increase in the group refractive index,  $n_g$ , which can lead to higher  $Q$ . Similarly, we assume that as the particle moves closer to the ASR metamaterial, this effectively increases the ambient group refractive index, leading to an increase in laser intensity. This behavior is directly related to the figure-of-merit (FOM). A nanoscale cavity is typically characterized by the FOM, which is proportional to the ratio of the  $Q$ -factor to the cubic power of the ambient refractive index, *i.e.*,  $Q/n^3$ . Thereby, the FOM may decrease with an increasing refractive index. Considering the above

analysis, we assume that the decreased trap stiffness enhancement factor at high trapping laser intensities (Figure 4c) may be due to a decrease in the FOM.

## Conclusions

An array of asymmetric split-rings with the ability to support a Fano resonance peak and boost near-field enhancement was fabricated in order to demonstrate a new platform for the next generation of optical trapping instruments. Trapping performance was investigated as a function of incident laser intensity and trapping wavelength. The scaled trapping efficiency of 8.65 fN/nm/mW for 20 nm polystyrene particles using a 930 nm trapping laser is the highest value reported for dielectric nanoparticle trapping. The mechanism underpinning the trap stiffness enhancement results from the ultra-small effective electromagnetic mode volume and the Purcell effect contribution. Our approach can be used to qualitatively understand the folding mechanism of biomolecules, such as proteins and nucleic acids, that is related to the evolution of various diseases and which could contribute to drug discoveries.

## Methods

### Sample Fabrication

An array of asymmetric split-rings (ASRs) was fabricated using focused ion beam (FIB-FEI Helios G3UC) milling on a 50-nm gold thin film (PHASIS, Geneva, BioNano) at 30 kV energy and 2 pA beam current. The metamaterial device, which was used for trapping experiments, consisted of 17 ( $x$ -direction) and 15 ( $y$ -direction) identical ASR units, *i.e.*, metamolecules.

### Experimental Set up

The optical tweezers consist of a tunable, continuous-wave (cw) Ti:Sapphire laser focused using a  $1.3\times$  numerical aperture (NA) oil immersion objective lens (OLYMPUS UPlanFL N



100 $\times$ ) onto the metamaterial device, which was mounted on an xyz-piezo nanopositioning stage. We controlled both the polarization and incident power of the trapping beam, which was limited to a maximum power of 10 mW at the sample plane. Detection of a trapping event was done by collecting the transmitted laser light through a 50 $\times$  objective lens (Nikon CF Plan) and sending it to an avalanche photodiode (APD430A/M, Thorlabs). A second APD was used to collect reflected laser light through an oil immersion objective lens. APD signals were recorded using a data acquisition board (DAQ) at a frequency of 100 kHz with LabVIEW. In order to calculate the trap stiffness, we only analyzed data for which the APD signal of the reflected laser light was in the opposite direction (step-like jump up or down) to the APD signal of the transmitted laser light (step-like jump down or up). This ensured that the step-like jump was due to an optical trapping event.

## Materials



The metamaterial device was attached to a cover glass with adhesive microscope spacers (Grace BioLabs, Sigma-Aldrich, GBL654002), forming a microwell. The microwell contained polystyrene (PS) particles with a mean diameter of 20 nm (ThermoFisher Scientific, F8786) in heavy water (D<sub>2</sub>O) with a 0.0625% mass concentration. A small amount of surfactant (Detergent Tween 20 with 0.1% volume concentration) was used to minimize aggregation. The microwell was mounted and fixed on top of a piezoelectric translation stage.

## Spectra Measurements

Transmission,  $T$ , and reflection,  $R$ , spectra of the metamaterial were obtained using a microspectrophotometer (MCRAIC 20/30 PV). The absorption,  $A$ , spectrum was determined from the following:  $A(\%) = 100(\%) - T(\%) - R(\%)$ .

## Corresponding authors

**Email:** sile.nicchormaic@oist.jp; v.g.truong@oist.jp

Domna G. Kotsifaki  :0000-0002-2023-8345 Viet Giang Truong  :0000-0003-3589-7850

Síle Nic Chormaic  :0000-0003-4276-2014

## Author Contributions

SNC and VGT conceived the experiments. DGK and VGT performed the experiments and analyzed the data. All authors discussed the results and contributed to the manuscript.

## Notes

The authors declare no competing financial interests.

## Acknowledgement

This work was supported by funding from Okinawa Institute of Science and Technology Graduate University. The authors are grateful to Nikitas Papasimakis for useful comments on the manuscript. The authors would like to thank Simon Peter Mekhail and Metin Ozer for technical assistance, Steven D. Aird for reviewing the manuscript and Emi Nakamura for general research support.

## Supporting Information Available

Additional figures, their descriptions and detailed discussions about: experimental set-up, multiple nanoparticle trapping, power spectral density analysis, Faxén’s correction, numerical simulations and  $Q$ -factor of the Fano resonance.

## References

- (1) Ritchie, R. H.; Arakawa, E. T.; Cowan, J. J.; Hamm, R. N. Surface-Plasmon Resonance Effect in Grating Diffraction. *Phys. Rev. Lett.* **1968**, *21*, 1530–1533.
- (2) Kravets, V. G.; Kabashin, A. V.; Barnes, W. L.; Grigorenko, A. N. Plasmonic Surface Lattice Resonances: A Review of Properties and Applications. *Chemical reviews* **2018**, *118*, 5912–5951.
- (3) Ebbesen, T. W.; Lezec, H. J.; Ghaemi, H. F.; Thio, T.; Wolff, P. A. Extraordinary optical transmission through sub-wavelength hole arrays. *Nature* **1998**, *391*, 667–669.
- (4) Kabashin, A. V.; Evans, P.; Pastkovsky, S.; Hendren, W.; Wurtz, G. A.; Atkinson, R.; Pollard, R.; Podolskiy, V. A.; Zayats, A. V. Plasmonic nanorod metamaterials for biosensing. *Nature Materials* **2009**, *8*, 867–871.
- (5) Gutha, R. R.; Sadeghi, S. M.; Sharp, C.; Wing, W. J. Biological sensing using hybridization phase of plasmonic resonances with photonic lattice modes in arrays of gold nanoantennas. *Nanotechnology* **2017**, *28*, 355504.
- (6) Li, J.; Ma, Y.; Gu, Y.; Khoo, I.-C.; Gong, Q. Large spectral tunability of narrow geometric resonances of periodic arrays of metallic nanoparticles in a nematic liquid crystal. *Applied Physics Letters* **2011**, *98*, 213101.
- (7) Niinomi, H.; Sugiyama, T.; Uda, S.; Tagawa, M.; Ujihara, T.; Miyamoto, K.; Omatsu, T. Plasmonic Trapping-Induced Crystallization of Acetaminophen. *Crystal Growth & Design* **2019**, *19*, 529–537.
- (8) Lee, H.; Hong, W.; Jeon, S.; Choi, Y.; Cho, Y. Electroactive Polypyrrole Nanowire Arrays: Synergistic Effect of Cancer Treatment by On-Demand Drug Release and Photothermal Therapy. *Langmuir* **2015**, *31*, 4264–4269.

- (9) Huang, X.; El-Sayed, I. H.; Qian, W.; El-Sayed, M. A. Cancer Cell Imaging and Photothermal Therapy in the Near-Infrared Region by Using Gold Nanorods. *Journal of the American Chemical Society* **2006**, *128*, 2115–2120.
- (10) Della Rocca, J.; Liu, D.; Lin, W. Nanoscale Metal–Organic Frameworks for Biomedical Imaging and Drug Delivery. *Accounts of Chemical Research* **2011**, *44*, 957–968.
- (11) Novotny, L.; Bian, R. X.; Xie, X. S. Theory of Nanometric Optical Tweezers. *Phys. Rev. Lett.* **1997**, *79*, 645–648.
- (12) Okamoto, K.; Kawata, S. Radiation Force Exerted on Subwavelength Particles near a Nanoaperture. *Phys. Rev. Lett.* **1999**, *83*, 4534–4537.
- (13) Kotsifaki, D. G.; Nic Chormaic, S. Plasmonic optical tweezers based on nanostructures: fundamentals, advances and prospects. *Nanophotonics* **2019**, *8*, 1227–1245.
- (14) Kotsifaki, D. G.; Kandyla, M.; Lagoudakis, P. G. Near-field enhanced optical tweezers utilizing femtosecond-laser nanostructured substrates. *Applied Physics Letters* **2015**, *107*, 211111.
- (15) Daly, M.; Sergides, M.; Nic Chormaic, S. Optical trapping and manipulation of micrometer and submicrometer particles. *Laser & Photonics Reviews* **2015**, *9*, 309–329.
- (16) Han, X.; Truong, V. G.; Prince, S. T.; Nic Chormaic, S. Sequential trapping of single nanoparticles using a gold plasmonic nanohole array. *Photonics Research* **2018**, *6*, 981–986.
- (17) Kotnala, A.; Gordon, R. Quantification of High-Efficiency Trapping of Nanoparticles in a Double Nanohole Optical Tweezer. *Nano Letters* **2014**, *14*, 853–856.
- (18) Mestres, P.; Berthelot, J.; Aćimović, S. S.; Quidant, R. Unraveling the optomechanical nature of plasmonic trapping. *Light: Science AND Applications* **2016**, *5*, e16092–e16092.

- (19) Saleh, A. A. E.; Dionne, J. A. Toward Efficient Optical Trapping of Sub-10-nm Particles with Coaxial Plasmonic Apertures. *Nano Letters* **2012**, *12*, 5581–5586.
- (20) Pang, Y.; Gordon, R. Optical Trapping of a Single Protein. *Nano Letters* **2012**, *12*, 402–406.
- (21) Al Balushi, A. A.; Kotnala, A.; Wheaton, S.; Gelfand, R. M.; Rajashekara, Y.; Gordon, R. Label-free free-solution nanoaperture optical tweezers for single molecule protein studies. *Analyst* **2015**, *140*, 4760–4778.
- (22) Roxworthy, B. J.; Ko, K. D.; Kumar, A.; Fung, K. H.; Chow, E. K. C.; Gang, L. L.; Fang, N. X.; Toussaint Jr, K. C. Application of Plasmonic Bowtie Nanoantenna Arrays for Optical Trapping, Stacking, and Sorting. *Nano Letters* **2012**, *12*, 796–801.
- (23) Juan, M. L.; Gordon, R.; Pang, Y.; Eftekhari, F.; Quidant, R. Self-induced back-action optical trapping of dielectric nanoparticles. *Nature Physics* **2009**, *5*, 915–919.
- (24) Yoo, D.; Gurunatha, K. L.; Choi, H.-K.; Mohr, D. A.; Ertsgaard, C. T.; Gordon, R.; Oh, S.-H. Low-Power Optical Trapping of Nanoparticles and Proteins with Resonant Coaxial Nanoaperture Using 10 nm Gap. *Nano Letters* **2018**, *18*, 3637–3642.
- (25) Jiang, Q.; Rogez, B.; Claude, J.; Baffou, G.; Wenger, J. Temperature Measurement in Plasmonic Nanoapertures Used for Optical Trapping. *ACS Photonics* **2019**, *6*, 1763–1773.
- (26) Sergides, M.; Truong, V. G.; Nic Chormaic, S. Highly tunable plasmonic nanoring arrays for nanoparticle manipulation and detection. *Nanotechnology* **2016**, *27*, 365301.
- (27) Han, X.; Truong, V. G.; Nic Chormaic, S. Efficient microparticle trapping with plasmonic annular apertures arrays. *Nano Futures* **2018**, *2*, 035007.
- (28) Chung, H. S.; McHale, K.; Louis, J. M.; Eaton, W. A. Single-Molecule Fluorescence

- Experiments Determine Protein Folding Transition Path Times. *Science* **2012**, *335*, 981–984.
- (29) Yunhui, P.; Emil, A.; Sankar, B. Structural Perspective on Revealing and Altering Molecular Functions of Genetic Variants Linked with Diseases. *International Journal of Molecular Sciences* **2019**, *20*.
- (30) Gámez, A.; Yuste-Checa, P.; Brasil, S.; Briso-Montiano, A.; Desviat, L. R.; Ugarte, M.; Pérez-Cerdá, C.; Pérez, B. Protein misfolding diseases: Prospects of pharmacological treatment. *Clinical Genetics* **2018**, *93*, 450–458.
- (31) Ozbay, E. The Magical World of Photonic Metamaterials. *Optics and Photonics News* **2008**, *19*, 22–27.
- (32) Luk'yanchuk, B.; Zheludev, N. I.; Maier, S. A.; Halas, N. J.; Nordlander, P.; Giessen, H.; Chong, T. C. The Fano resonance in plasmonic nanostructures and metamaterials. *Nature Materials* **2010**, *9*, 707–715.
- (33) Soukoulis, C. M.; Wegener, M. Past achievements and future challenges in the development of three-dimensional photonic metamaterials. *Nature Photonics* **2011**, *5*, 523–530.
- (34) Chihhui, W.; Khanikaev, A. B.; Adato, R.; Arju, N.; Ali, A. Y.; Altug, H.; Shvets, G. Fano-resonant asymmetric metamaterials for ultrasensitive spectroscopy and identification of molecular monolayers. *Nature Materials* **2012**, *11*, 69–75.
- (35) Papasimakis, N.; Zheludev, N. I. Metamaterial-Induced Transparency: Sharp Fano Resonances and Slow Light. *Optics and Photonics News* **2009**, *20*, 22–27.
- (36) Alitalo, P.; Tretyakov, S. Electromagnetic cloaking with metamaterials. *Materials Today* **2009**, *12*, 22–29.
- (37) Zheludev, N. I.; Prosvirnin, S. L.; Papasimakis, N.; Fedotov, V. A. Lasing spaser. *Nature Photonics* **2008**, *2*, 351.

- (38) Vahala, K. J. Optical microcavities. *Nature* **2003**, *424*, 839–846.
- (39) Fedotov, V. A.; Rose, M.; Prosvirnin, S. L.; Papasimakis, N.; Zheludev, N. I. Sharp Trapped-Mode Resonances in Planar Metamaterials with a Broken Structural Symmetry. *Physical Review Letters* **2007**, *99*, 147401.
- (40) Halas, N. J.; Lal, S.; Chang, W.-S.; Link, S.; Nordlander, P. Plasmons in Strongly Coupled Metallic Nanostructures. *Chemical Reviews* **2011**, *111*, 3913–3961.
- (41) Cao, T.; Mao, L.; Qiu, Y.; Lu, L.; Banas, A.; Banas, K.; Simpson, R. E.; Chui, H.-C. Fano Resonance in Asymmetric Plasmonic Nanostructure: Separation of Sub-10 nm Enantiomers. *Advanced Optical Materials* **2019**, *7*, 1801172.
- (42) Fedotov, V. A.; Papasimakis, N.; Plum, E.; Bitzer, A.; Walther, M.; Kuo, P.; Tsai, D. P.; Zheludev, N. I. Spectral Collapse in Ensembles of Metamolecules. *Phys. Rev. Lett.* **2010**, *104*, 223901.
- (43) Chen, Y.-F.; Serey, X.; Sarkar, R.; Chen, P.; Erickson, D. Controlled Photonic Manipulation of Proteins and Other Nanomaterials. *Nano Letters* **2012**, *12*, 1633–1637.
- (44) Xu, Z.; Song, W.; Crozier, K. B. Direct Particle Tracking Observation and Brownian Dynamics Simulations of a Single Nanoparticle Optically Trapped by a Plasmonic Nanoaperture. *ACS Photonics* **2018**, *5*, 2850–2859.
- (45) Chen, C.; Juan, M. L.; Li, Y.; Maes, G.; Borghs, G.; Van Dorpe, P.; Quidant, R. Enhanced Optical Trapping and Arrangement of Nano-Objects in a Plasmonic Nanocavity. *Nano Letters* **2012**, *12*, 125–132.
- (46) Hansen, P. M.; Bhatia, V. K.; Harrit, N.; Oddershede, L. Expanding the Optical Trapping Range of Gold Nanoparticles. *Nano Letters* **2005**, *5*, 1937–1942.
- (47) Rohrbach, A. Stiffness of Optical Traps: Quantitative Agreement between Experiment and Electromagnetic Theory. *Phys. Rev. Lett.* **2005**, *95*, 168102.

- (48) Verschueren, D.; Shi, X.; Dekker, C. Nano-Optical Tweezing of Single Proteins in Plasmonic Nanopores. *Small Methods* **2019**, *3*, 1800465.
- (49) Nicoli, F.; Verschueren, D.; Klein, M.; Dekker, C.; Jonsson, M. P. DNA Translocations through Solid-State Plasmonic Nanopores. *Nano Letters* **2014**, *14*, 6917–6925.
- (50) Ndukaife, J. C.; Kildishev, A. V.; Nnanna, A. G. A.; Shalaev, V. M.; Wereley, S. T.; Boltasseva, A. Long-range and rapid transport of individual nano-objects by a hybrid electrothermoplasmonic nanotweezer. *Nature Nanotechnology* **2015**, *11*, 53.
- (51) Ndukaife, J. C.; Mishra, A.; Guler, U.; Nnanna, A. G. A.; Wereley, S. T.; Boltasseva, A. Photothermal Heating Enabled by Plasmonic Nanostructures for Electrokinetic Manipulation and Sorting of Particles. *ACS Nano* **2014**, *8*, 9035–9043.
- (52) Ndukaife, J. C.; Xuan, Y.; Nnanna, A. G. A.; Kildishev, A. V.; Shalaev, V. M.; Wereley, S. T.; Boltasseva, A. High-Resolution Large-Ensemble Nanoparticle Trapping with Multifunctional Thermoplasmonic Nanohole Metasurface. *ACS Nano* **2018**, *12*, 5376–5384.
- (53) Tanaka, K.; Plum, E.; Ou, J. Y.; Uchino, T.; Zheludev, N. I. Multifold Enhancement of Quantum Dot Luminescence in Plasmonic Metamaterials. *Physical Review Letters* **2010**, *105*, 227403.
- (54) Corcoran, B.; Monat, C.; Grillet, C.; Moss, D. J.; Eggleton, B. J.; White, T. P.; O’Faolain, L.; Krauss, T. F. Green light emission in silicon through slow-light enhanced third-harmonic generation in photonic-crystal waveguides. *Nature Photonics* **2009**, *3*, 206–210.
- (55) Scullion, M. G.; Arita, Y.; Krauss, T. F.; Dholakia, K. Enhancement of optical forces using slow light in a photonic crystal waveguide. *Optica* **2015**, *2*, 816–821.



- (56) Papasimakis, N.; Fedotov, V. A.; Zheludev, N. I.; Prosvirnin, S. L. Metamaterial Analog of Electromagnetically Induced Transparency. *Phys. Rev. Lett.* **2008**, *101*, 253903.

## Graphical TOC Entry

